oral

Article

Impact of Metal Artifact Reduction on the Diagnosis of Peri-Implant Defects Around Zirconia and Titanium Implants: A CBCT Pilot Study

Mahsa Moannaei [1], Mojdeh Mehdizadeh [2], Farnaz Mirrashidi [3,*], Mohammad Hossein Manouchehri [4], Sepehr Naghdi [5], Amirhossein Moaddabi [6], Nima Malek Hosseini [7], Gianrico Spagnuolo [8,9,*], Francesco Giordano [10,†] and Parisa Soltani [2,8,†]

1 Department of Oral and Maxillofacial Radiology, School of Dentistry, Hormozgan University of Medical Sciences, Bandar Abbas 7916613885, Iran; moannaei_m@yahoo.com
2 Department of Oral and Maxillofacial Radiology, Dental Implants Research Center, Dental Research Institute, School of Dentistry, Isfahan University of Medical Sciences, Isfahan 8174673461, Iran; mehdizadeh@dnt.mui.ac.ir (M.M.); parisa.soltani@live.com (P.S.)
3 Department of Oral and Maxillofacial Radiology, School of Dentistry, Alborz University of Medical Sciences, Karaj 3198684868, Iran
4 Department of Oral and Maxillofacial Surgery, School of Dentistry, Isfahan University of Medical Sciences, Isfahan 8174673461, Iran; manouchehri@dnt.mui.ac.ir
5 Student Research Committee, School of Dentistry, Isfahan University of Medical Sciences, Isfahan 8174673461, Iran; sepehrnaghdi@gmail.com
6 Department of Oral and Maxillofacial Surgery, Dental Research Center, Mazandaran University of Medical Sciences, Sari 4816895475, Iran; a.moaddabi@mazums.ac.ir
7 Department of Oral and Maxillofacial Surgery, School of Dentistry, Tehran University of Medical Sciences, Tehran 1439955991, Iran; malekhosseini@tums.ac.ir
8 Department of Neurosciences, Reproductive and Odontostomatological Sciences, University of Naples 'Federico II', 80131 Naples, Italy
9 Saveetha Dental College and Hospitals, Saveetha Institute of Medical and Technical Sciences, Saveetha University, Chennai 600077, Tamil Nadu, India
10 Department of Medicine, Surgery and Dentistry, University of Salerno, 84084 Salerno, Italy; fgiordano@unisa.it
* Correspondence: fs.mirrashidi@gmail.com (F.M.); gspagnuo@unina.it (G.S.)
† These authors contributed equally to this work.

Highlights

What are the main findings?

- For titanium implants, metal artifact reduction (MAR) had no effect on diagnostic performance.
- For zirconia implants, MAR improved sensitivity for small fenestrations but reduced specificity.

What are the implications of the main findings?

- MAR is unnecessary for evaluating peri-implant defects around titanium implants.
- When imaging zirconia implants, clinicians must balance higher sensitivity against lower specificity when activating MAR.

Academic Editor: Massimo Del Fabbro

Received: 22 March 2026
Revised: 18 June 2026
Accepted: 26 June 2026
Published: 3 July 2026

Abstract

Background/Objectives: Metal artifacts from dental implants degrade CBCT image quality and may impair detection of peri-implant bone defects. Zirconia implants produce stronger artifacts than titanium due to its higher atomic number. This study evaluated the impact of a native MAR algorithm (SMARF) on CBCT detection of buccal fenestration and dehiscence of varying sizes adjacent to zirconia versus titanium implants. **Methods**: In this ex vivo

 https://doi.org/10.3390/oral6040083

pilot study, two 4 mm × 12 mm implants (one titanium and one zirconia) were implanted in a dry human mandible. Artificial fenestration and dehiscence defects were created at the buccal surface of right and left premolar regions, in three sizes (small 2 mm × 2 mm× 1 mm; medium 2 mm × 4 mm× 1 mm; large 2 mm × 6 mm× 1 mm). Scans were acquired with a Papaya 3D (Genoray) CBCT using a single-tooth FOV (4 cm× 4 cm × 5 cm), 83 kVp, 10 mA, 0.1 mm voxel; each condition was imaged with MAR on and off (six repeats each). Two trained observers scored defect presence on a five-point Likert scale. Sensitivity, specificity, inter- and intraobserver agreement (Cohen's kappa), and comparisons across conditions were calculated. **Results**: Interobserver κ = 0.65 (substantial); intraobserver κ = 0.87–1.00 (excellent). For titanium implants, sensitivity and specificity were 100% across all defect types, sizes, and MAR settings. For zirconia implants, fenestration sensitivity with MAR off increased with size (small 50%, medium 75%, large 100%); MAR on raised sensitivity to 100% for all sizes, with a significant improvement for small fenestrations ($p = 0.005$). Dehiscence sensitivity for zirconia was 100% across sizes and MAR conditions. Specificity for zirconia defects was 83.3% with MAR off and decreased to 66.6% with MAR on ($p = 0.07$). **Conclusions**: With the Papaya 3D system used in this pilot study, MAR was unnecessary for defect detection adjacent to titanium implants but affected performance for zirconia implants: MAR increased sensitivity for small fenestrations while reducing specificity (although not statistically significant). Clinicians should weigh the sensitivity–specificity trade off when applying MAR around zirconia implants.

Keywords: CBCT; artifacts; implants; fenestration; dehiscence; titanium; zirconia

1. Introduction

Peri-implantitis is an irreversible infectious condition around dental implants that can ultimately lead to implant failure, with reported prevalence exceeding 20% [1–3]. Local risk factors such as inadequate peri-implant bone volume and implant malpositioning markedly increase the likelihood of bone defects around implants, which in turn compromise primary stability and osseointegration. Fenestration describes a localized loss of cortical bone over the mid-root region while the marginal bone remains intact, while dehiscence denotes loss of the marginal bone and absence of cervical bone support. Both defect types predispose to peri-implantitis and implant failure, so early and reliable detection is essential to preserve long-term implant success [4].

Cone beam computed tomography (CBCT) provides three-dimensional visualization of buccal and lingual cortical plates and enables assessment of marginal bone contour and intraosseous defects that are not visible on conventional radiographs [5]. Nevertheless, CBCT performance around dental implants is challenged by metal artifacts. Implant materials with high atomic numbers produce beam hardening and photon starvation artifacts that generate streaks and dark shadows, degrading image quality and impairing diagnostic accuracy [6].

Zirconia implants offer aesthetic and biological advantages, such as tooth-like color, biocompatibility, favorable osseointegration potential, and reduced plaque accumulation, making them an attractive alternative to titanium, especially in patients with thin mucosal phenotypes [7]. However, the higher atomic number of zirconia increases the severity of metal artifacts in CBCT, further compromising image detail [8].

Manufacturers propose two main strategies to mitigate artifacts: altering acquisition parameters (FOV, voxel size, kVp, mA, exposure time) and applying metal artifact reduction (MAR) algorithms during reconstruction [9–11]. Exposure adjustments can increase

https://doi.org/10.3390/oral6040083

radiation dose and must be used cautiously [12]. MAR algorithms mathematically modify raw or reconstructed data to reduce hyper- and hypodense streaks, but they require longer reconstruction times and greater computing power and may, in some situations, reduce diagnostic accuracy [13]. Published studies report inconsistent effects of MAR and imaging parameters on the detection of fenestration and dehiscence, and differences have been observed between titanium and zirconia implants in sensitivity and specificity [1,10,14,15].

Given the increasing clinical use of zirconia implants and the central role of CBCT in peri-implant bone assessment, there is a clear need to evaluate how MAR affects artifact severity and the diagnostic performance of CBCT for bone defects of varying sizes adjacent to zirconia implants. This study aimed to investigate the impact of MAR activation on metal artifacts produced by zirconia implants and on CBCT accuracy for detecting fenestration and dehiscence of different dimensions.

2. Materials and Methods

2.1. Implants and Specimen Preparation

In this ex vivo pilot study, a dry human mandible retrieved from the radiology department archive was used to ensure consistent anatomical conditions across defect sizes. Two cylindrical dental implants (titanium and zirconia; Bredent, Senden, Germany), both 4 mm × 12 mm, were used. Implant osteotomies were prepared following the manufacturer's standard drilling protocol. Implant sites were located in the posterior region: the right second premolar site and the left first premolar site (Figure 1a–d). Defects were created, using a round bur with a 2 mm diameter, on the buccal cortical plate at the two implant sites to simulate fenestration and dehiscence lesions. Defect locations and dimensions were determined with reference to CBCT-derived cortical thickness measurements.

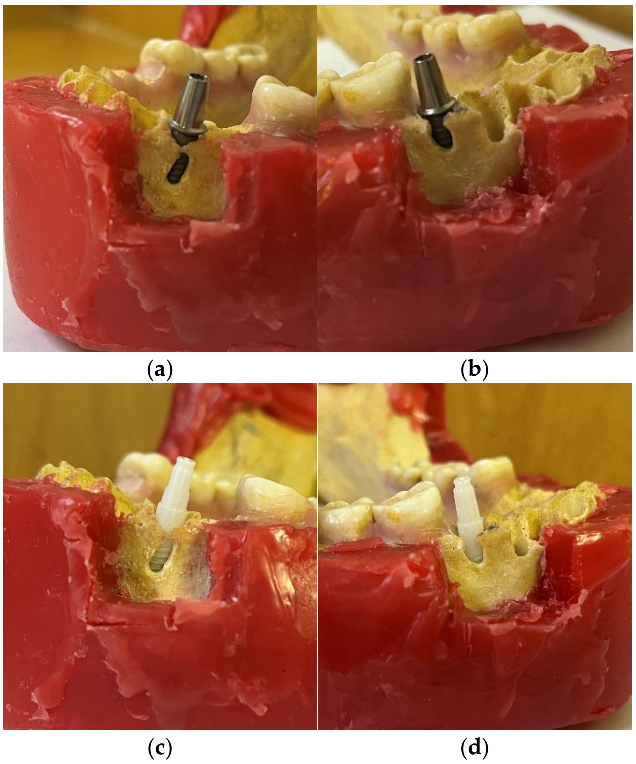

Figure 1. Specimens demonstrating (**a**) fenestration defect adjacent to a titanium implant; (**b**) dehiscence defect adjacent to a titanium implant; (**c**) fenestration defect adjacent to a zirconia implant; and (**d**) dehiscence defect adjacent to a zirconia implant.

Small-size group:

- Fenestration (left first premolar, coronal third of buccal cortical plate): width 2 mm × height 2 mm × depth 1 mm; positioned 2 mm apical to the marginal cortex.
- Dehiscence (right second premolar, marginal buccal cortical plate): width 2 mm × height 2 mm × depth 1 mm.

Medium-size group:

- Fenestration: 2 mm × 4 mm × 1 mm.
- Dehiscence: 2 mm × 4 mm × 1 mm.

Large-size group:

- Fenestration: 2 mm × 6 mm × 1 mm.
- Dehiscence: 2 mm × 6 mm × 1 mm.

All buccal surfaces of the mandible were coated with 1 cm of acrylic resin to simulate soft-tissue coverage [16]. Control images were acquired for (1) the mandible with implants but before creation of defects (control without defect), and (2) mandible without implants (control without implant). Each scanning condition (every defect size and each control condition) was acquired six times.

2.2. CBCT Acquisition, Reconstruction, and Viewing

CBCT scans were obtained with a Papaya 3D unit (Genoray, Seoul, Republic of Korea) using a single-tooth field of view (4 cm × 4 cm × 5 cm). Scanning parameters were constant across all acquisitions: exposure time 7.7 s, 83 kVp, 10 mA, voxel size 0.1 mm. Images were reconstructed in two MAR algorithm settings using the native algorithm:

1. MAR On (post-processing enabled);
2. MAR Off (no MAR applied).

Volume reconstruction and image export were performed using OnDemand software version 2015 (CyberMed, Daejeon, Republic of Korea). Image assessment was carried out in a quiet, dimly lit room on a 21-inch medical-grade monitor. Observers were allowed to use all available viewing tools and layouts in the software; no time limit was imposed for image interpretation (Figure 2a–h).

Two trained observers performed the image assessments: a final-year radiology resident and a board-certified radiologist with 3 and 7 years of CBCT analysis experience, respectively. Prior to the study readings, a calibration session was held during which five independent mandibular bone-defect cases (fenestration and dehiscence), not included in the study set, were reviewed jointly.

Images were presented to observers in random order. The observers were blinded to all imaging conditions, including implant type, MAR setting, defect type, and defect size. For each image the observer recorded a score for the presence of a buccal cortical defect based on the following 5-point Likert scale:

1 = Definitely absent;
2 = Probably absent;
3 = Uncertain;
4 = Probably present;
5 = Definitely present.

2.3. Statistical Analysis

The required total sample size for this study was estimated at 324 specimens (each combination including 6 repetitions), calculated using PASS 2025 Power Analysis and Sample Size Software (NCSS, LLC, Kaysville, UT, USA, ncss.com/software/pass (accessed on 10 March 2025)) to detect a minimum medium effect size of 0.25, with a type I error rate of 5% and statistical power of 80%. All readings were recorded on standardized data sheets linking case identifiers, scan parameters (MAR On/Off, defect size), implant material/site, and the observer's classification. To assess intraobserver agreement, 20% of the image set was randomly selected and re-evaluated by each observer after a two-week interval. Cohen's kappa test was used to assess intraobserver and interobserver agreement. Sensitivity and specificity values were calculated for the different conditions. Chi-square tests were performed for comparisons using IBM SPSS Statistics version 27 (IBM Statistics, Armonk, NY, USA). A significance level of 0.05 was considered.

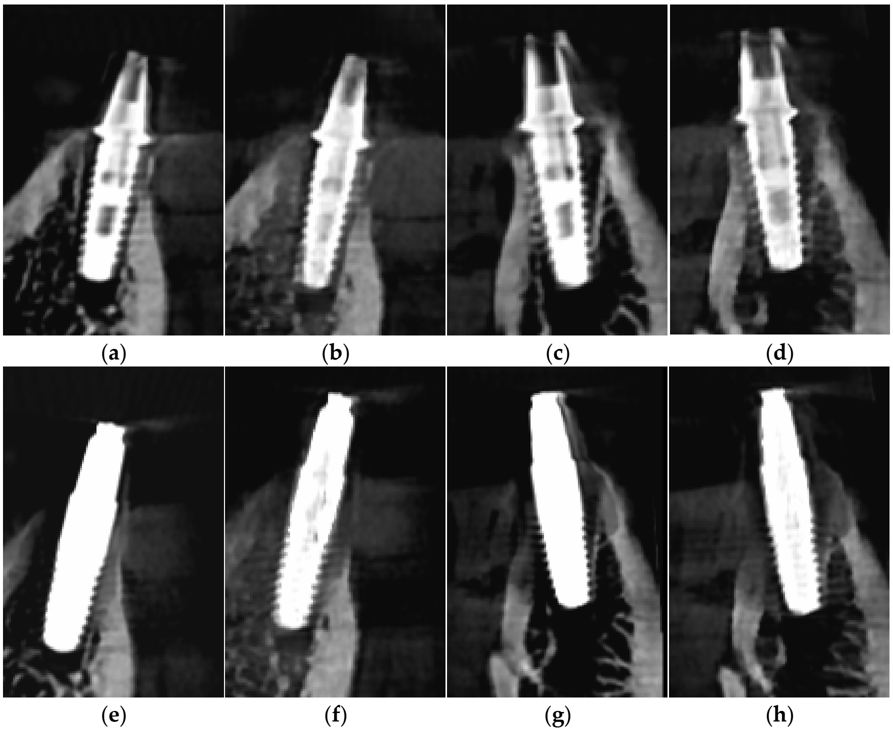

Figure 2. Cross-sectional CBCT images depicting (**a**) small fenestration defect adjacent to a titanium implant in MAR Off mode; (**b**) small fenestration defect adjacent to a titanium implant in MAR On mode; (**c**) small dehiscence defect adjacent to a titanium implant in MAR Off mode; (**d**) small dehiscence defect adjacent to a titanium implant in MAR On mode; (**e**) small fenestration defect adjacent to a zirconia implant in MAR Off mode; (**f**) small fenestration defect adjacent to a zirconia implant in MAR On mode; (**g**) small dehiscence defect adjacent to a zirconia implant in MAR Off mode; and (**h**) small dehiscence defect adjacent to a zirconia implant in MAR On mode.

3. Results

The interobserver Cohen's kappa was 0.65, indicating substantial agreement. The intraobserver agreements ranged between 0.87 and 1.00, indicating excellent agreement.

For titanium implants, sensitivity and specificity were 100% across all defect types and sizes, with MAR off or on.

For zirconia implants, the sensitivity for detecting small fenestration defects with MAR off was 50%, for medium size 75%, and for large size 100%. With MAR on, sensitivity for fenestration reached 100% at all sizes, and this difference was statistically significant for the small-size group ($p = 0.005$), while not significant for medium ($p = 0.06$) and large sizes ($p > 0.99$). Sensitivity for detecting dehiscence defects adjacent to zirconia implants was 100% for all sizes with both MAR off and MAR on.

Specificity for detecting dehiscence and fenestration defects at all sizes adjacent to zirconia implants was 83.3% with MAR off. Specificity decreased to 66.6% with MAR on; this reduction was not statistically significant ($p = 0.07$). With MAR off, sensitivity

https://doi.org/10.3390/oral6040083

for detecting fenestration defects adjacent to zirconia implants increased as defect size increased, and the increase between the small- and large-size groups was statistically significant (Table 1). With MAR off, detecting fenestration defects adjacent to zirconia implants was more difficult than detecting dehiscence defects, and this difference was statistically significant ($p = 0.046$).

Table 1. Comparison of diagnostic sensitivity and specificity according to defect type and defect size in zirconia implants under MAR on and off imaging conditions.

Implant Type	Defect Type	Defect Size	MAR Off		MAR On	
			Sensitivity	Specificity	Sensitivity	Specificity
Zirconia	Fenestration	Small	50%	83.3%	100%	66.6%
		Medium	75%	83.3%	100%	66.6%
		Large	100%	83.3%	100%	66.6%
	Dehiscence	Small	100%	83.3%	100%	66.6%
		Medium	100%	83.3%	100%	66.6%
		Large	100%	83.3%	100%	66.6%

MAR: metal artifact reduction.

4. Discussion

In this ex vivo pilot CBCT study, diagnostic detection of peri-implant defects around titanium implants showed excellent performance: sensitivity and specificity were 100% regardless of defect type, size, or MAR status. Around zirconia implants, detection of dehiscence demonstrated consistently high sensitivity but relatively lower specificity. Detection of small fenestration defects adjacent to zirconia implants was poor with MAR off, but sensitivity increased significantly with MAR on. Overall, dehiscence was more readily detected than fenestration around zirconia implants.

The use of MAR remains a controversial topic in the literature [17]. Many studies that examined the effect of MAR on image quality and contrast-to-noise ratio (CNR) have shown that MAR markedly reduces metal artifacts [8,11,18]. However, diagnostically, while some reports found that MAR improves detection [15], others found no effect on diagnostic performance for identifying dehiscence or fenestration [19].

The present study evaluated the influence of multiple variables on CBCT detection of peri-implant defects, including implant type, defect type, defect size, and MAR status (On vs. Off). Our results showed that titanium implants did not negatively affect defect detection in any condition or defect type and significantly allowed better detection than zirconia implants. In contrast, small fenestration defects adjacent to zirconia implants had lower sensitivity, which increased significantly when MAR was applied. The reduced specificity observed around zirconia implants indicates that correctly identifying defect-free sites remained problematic even with MAR enabled. Below, we examine each variable and its effects in more detail:

4.1. Implant Type

Rapid advances in CBCT scanners and the submillimetric resolution of three-dimensional CBCT images have increased the use of this imaging technology. Although CBCT is widely used for many maxillofacial tasks, it has drawbacks such as artifacts produced by high-atomic-number materials that degrade image quality. In the present study, titanium implants had a significantly smaller negative effect on correct diagnosis. This finding is consistent with several studies (e.g., Kuusisto et al. [1], Fonetenele et al. [10], Bayrak et al. [15], Demirturk Kocasarak et al. [20]), which showed that zirconium implants produce more metal artifact than titanium implants because of their higher atomic number (Z = 40 versus Z = 22), leading to adverse diagnostic effects. Therefore, it should be emphasized that image analysis requires greater caution in the presence of zirconia implants because they create more artifacts and may lead to false image interpretations.

4.2. Defect Type and Size

In the present pilot study, detection of defects adjacent to titanium implants, regardless of defect type or size, showed 100% sensitivity and specificity with MAR both on and off. Detection of dehiscence adjacent to zirconia implants also demonstrated high sensitivity with MARA on and off, but relatively lower specificity. By contrast, detection of small fenestration defects next to zirconia implants showed low sensitivity. Overall, diagnostic performance for dehiscence was significantly better than for fenestration.

Consistent with our findings, Fontenele et al. [10] reported that changes in kVp and MAR tools had no effect on detection of bony dehiscence in either the buccal or lingual cortex. They also observed higher sensitivity but lower specificity in the presence of zirconia implants compared with titanium, independent of exposure parameters. Likewise, Sheikhi et al. [21] reported sensitivity above 0.91 for detecting dehiscence near titanium implants and above 0.81 for detecting fenestration.

In contrast, De-Azevedo et al. [19] reported sensitivity for detecting dehiscence near titanium implants ranging from 0.28 to 0.41 and for fenestration from 0.62 to 0.66. Freire et al. [17] reported higher sensitivity for fenestration detection next to zirconia implants compared with dehiscence, although that difference was not statistically significant. These findings are not consistent with the present study. The discrepancies can be explained by methodological differences among studies; for example, use of bovine rib bone blocks (which have greater cortical thickness than the human mandible used in the present study), placement of fenestration defects in the apical third in other studies versus small fenestrations placed in the coronal third of the human mandible in the present study, and different defect sizes (e.g., 2.5 mm in the other study, larger than our small defect).

Studies indicate that adequate bone thickness is important for better detection of peri-implant defects. Key factors affecting CBCT accuracy for measuring experimental bone defects include defect size and the presence of artifacts [22]. In general, the defect location, defect size, voxel size, CBCT device and exposure parameters, the MAR algorithm used, and the radiologist's experience are all factors that may influence defect detection.

In our study, detection of small fenestration defects (2 mm $\times$ 2 mm $\times$ 1 mm) showed lower sensitivity, which increased with defect size; the difference between small and large sizes was statistically significant. Consistent with our results, Kamburoğlu et al. [23] created dehiscence defects of varying sizes around titanium implants placed in the mandible and classified them by depth and width as small (1–3 mm), medium (3–5 mm), and large (>5 mm). They found that smaller defects had lower diagnostic accuracy compared with medium and large defects. Similar outcomes were reported by Hilgenfeld et al. [24] and Pinheiro et al. [25]: larger peri-implant bone defects were generally measured with greater accuracy than smaller defects, and the ability to detect these defects improved progressively as their size increased.

4.3. MAR Condition

The present study showed that activation or deactivation of the MAR algorithm (called SMARF in the CBCT scanner used in this study) on the Papaya 3D Genoray system did not affect defect detection in images of titanium implants, regardless of defect type or size. Images of dehiscence and fenestration defects adjacent to zirconia implants showed low specificity, which decreased further when MAR was enabled; however, this difference

https://doi.org/10.3390/oral6040083

was not statistically significant. Sensitivity for detecting fenestration defects around zirconia implants increased with defect size and with MAR activation, and this increase was statistically significant.

Overall, MAR algorithms are classified into five categories: (1) physical-modeling-based approaches, (2) projection-completion-based approaches, (3) dual-energy-based approaches, (4) iterative-reconstruction-based approaches, and (5) deep-learning-based approaches [13]. All aim to correct gray-value distortions caused by metal artifacts. The effectiveness of each MAR type can vary depending on whether it is applied pre-scan or post-scan and on the clinical or diagnostic application (e.g., defect detection, root fracture detection, assessment of implant-related nerve injury), so different MAR implementations may perform differently. The Papaya 3D unit used in the current study incorporates a proprietary metal artifact reduction tool termed SMARF™ (Smart Metal Artifact Reduction Function). In this system, SMARF is applied exclusively after image acquisition and reconstruction, functioning as a post-processing, image-domain correction step.

Bayrak et al. [15] evaluated the effects of MAR and an adaptive image noise optimizer (AINO) on the accuracy of dehiscence detection (3–4 mm diameter) adjacent to three implant types (titanium, zirconia, and titanium–zirconia) in a sheep mandibular model. Using a Planmeca Promax 3-D Max scanner (90 kVp, 10 mA, 0.1 mm voxel, 5 cm × 5.5 cm FOV, 12 s), they reported higher diagnostic accuracy for scans with MAR (with or without AINO) compared with scans without MAR.

Shahmirzadi et al. [18] assessed artifacts generated by a Planmeca ProMax® 3D Max CBCT unit (Planmeca Oy, Helsinki, Finland) using three MAR modes (pre-scan MAR, post-scan MAR, and no MAR). Their exposure parameters were 84–90 kVp, 8 mA, 200 µm voxel, 8 cm × 8 cm FOV, 12 s. All three analyses showed that MAR reduced artifacts, with no significant difference between pre- and post-activation.

Soltani et al. [13] examined the effect of MAR activation on the detection of implant-related injuries to the inferior alveolar canal using a Galileos scanner (85 kVp, 21 mAs, 280 µm voxel, 15 cm × 15 cm FOV, Sirona, Bensheim, Germany) and reported that MAR affected the diagnostic accuracy of CBCT images, though the effect was not statistically significant—findings consistent with the present study.

Conversely, Salemi et al. [26] evaluated MAR effectiveness on ProMax 3D (84 kVp, 14 mA, 200 µm voxel, 7.5 cm × 11 cm FOV, 12 s) and Cranex 3D (90 kVp, 10 mA, 200 µm voxel, 6 cm × 8 cm FOV, 14 s, Soredex, Helsinki, Finland) scanners for detecting small defects (2 mm diameter) of fenestration and dehiscence around titanium implants placed in bovine rib. They found that MAR significantly reduced diagnostic accuracy for both defect types.

Nomier et al. [14] studied low-dose CBCT (Green CT, Vatech Co., Ltd., Hwaseong, South Korea; 90 kVp, 2 mA, 0.08 mm voxel, 5 cm × 5 cm FOV, 9.5 s) with MAR for detecting dehiscence and fenestration around titanium implants in bovine ribs and reported no difference in AUC or diagnostic values when MAR was off; however, MAR use reduced diagnostic ability, particularly for dehiscence.

Fontenele et al. [10] found that applying MAR on a Picasso Trio unit (90 kV, 5 mA, 0.2 mm voxel, 8 cm × 5 cm FOV, Vatech Co., Ltd., Hwaseong, South Korea) did not affect the detection of 3 mm dehiscence around zirconia implants placed in the mandible. Freir et al. [17] similarly reported no MAR effect on detecting dehiscence and fenestration (2.5 mm diameter) around zirconia implants placed in bovine ribs using a Cranex3D unit (70–90 kV, 8 mA, 0.13 mm voxel, 4 cm × 4 cm FOV, 19 s). These findings differ from the present study. A critical point when reviewing the MAR literature is methodological heterogeneity: differences in the dental material studied, the MAR implementation, and the CBCT imaging systems used [27].

https://doi.org/10.3390/oral6040083

Broadly, MAR studies fall into two groups: those evaluating MAR's effect on image quality and CNR, and those assessing MAR's effect on diagnostic accuracy. While the first group consistently shows that MAR markedly reduces metal artifacts and improves image quality [8,11,18], the second group reports heterogeneous and sometimes conflicting diagnostic outcomes. This variability likely reflects differences in study design, including implant materials, defect characteristics, CBCT systems, MAR implementations, and evaluation criteria. Therefore, although MAR reliably enhances image appearance, its influence on diagnostic accuracy may vary across experimental settings and, in some circumstances, may even reduce diagnostic performance [26].

This pilot study evaluates technical diagnostic performance rather than biological variability. The controlled ex vivo design, using a single dry human mandible and two implants, allowed for the precise standardization of defect size, defect location, implant material, and imaging parameters, thereby isolating the effects of MAR activation without the confounding influence of inter-patient anatomical differences. Although the defects of different sizes were created sequentially in the same mandible, each represented a distinct diagnostic condition with unique cortical discontinuity characteristics. Nonetheless, the ex vivo model cannot fully reproduce in vivo factors such as heterogeneous bone density, variable soft-tissue thickness, anatomical complexity, and patient-related motion, all of which may influence artifact expression and diagnostic performance. Additionally, the artificially created defects, while standardized, may differ in morphology and border characteristics from naturally occurring peri-implant defects [10]. The very high sensitivity and specificity observed for titanium implants should be interpreted within the controlled conditions of this ex vivo model. Titanium produces comparatively mild artifacts on this CBCT system, and the preserved cortical boundaries in the dry mandible facilitated clear visualization of the buccal plate. Moreover, titanium served as a reference condition against which the diagnostic challenges posed by zirconia implants could be contrasted. The absence of biological heterogeneity, such as differences in bone density, soft-tissue attenuation, and patient-related motion, further reduces sources of diagnostic uncertainty that are commonly encountered in vivo. Therefore, although the findings provide valuable insight into MAR performance around zirconia and titanium implants within this CBCT system, clinical studies are required to validate these results under real patient conditions.

5. Conclusions

Given the CBCT system used in this pilot study (Papaya 3D, Genoray), applying the MAR algorithm was not necessary for detecting defects adjacent to titanium implants. However, using MAR for defects adjacent to zirconia implants reduces specificity (more false positive detections) and increases sensitivity (fewer false-negative detections) for small fenestration defects; however, only the increase in sensitivity was statistically significant. Although MAR activation may enhance the detection of small fenestration defects, it can also increase the likelihood of false positive findings. Therefore, clinicians should weigh the sensitivity–specificity trade off when applying MAR around zirconia implants. Further studies are needed to evaluate the diagnostic accuracy and clinical reliability of MAR.

Author Contributions: Conceptualization, F.M. and P.S.; methodology, F.M., P.S., S.N. and M.H.M.; software, S.N. and M.M. (Mojdeh Mehdizadeh); validation, F.M., P.S., and F.G.; formal analysis, M.M. (Mahsa Moannaei) and N.M.H.; resources, G.S. and M.M. (Mojdeh Mehdizadeh); data curation, F.G. and P.S.; visualization, S.N. and A.M.; supervision, G.S. and M.M. (Mojdeh Mehdizadeh); project administration, F.M. and A.M.; funding acquisition, M.M. (Mojdeh Mehdizadeh); writing—original draft preparation, F.M., P.S. and A.M.; writing—review and editing, all authors. All authors have read and agreed to the published version of the manuscript.

Funding: This research was funded by Isfahan University of Medical Sciences, grant number 3403230.

Institutional Review Board Statement: This ex vivo study was approved by the Research Ethics Committee of Isfahan University of Medical Sciences (protocol code IR.MUI.DHMT.REC.1403.084).

Informed Consent Statement: Not applicable.

Data Availability Statement: The data presented in this study are available on request from the corresponding authors.

Conflicts of Interest: The authors declare no conflicts of interest.

Abbreviations

The following abbreviations are used in this manuscript:

MAR	Metal Artifact Reduction
CBCT	Cone Beam Computed Tomography
AINO	Adaptive Image Noise Optimizer

References

1. Kuusisto, N.; Abushahba, F.; Syrjänen, S.; Huumonen, S.; Vallittu, P.; Närhi, T. Zirconia implants interfere with the evaluation of peri-implant bone defects in cone beam computed tomography (CBCT) images even with artifact reduction, a pilot study. *Dentomaxillofac. Radiol.* **2023**, *52*, 20230252. [CrossRef] [PubMed]
2. Derks, J.; Tomasi, C. Peri-implant health and disease. A systematic review of current epidemiology. *J. Clin. Periodontol.* **2015**, *42*, S158–S171. [CrossRef] [PubMed]
3. Lee, C.-T.; Huang, Y.-W.; Zhu, L.; Weltman, R. Prevalences of peri-implantitis and peri-implant mucositis: Systematic review and meta-analysis. *J. Dent.* **2017**, *62*, 1–12. [PubMed]
4. Severi, M.; Simonelli, A.; Farina, R.; Tu, Y.K.; Lan, C.H.; Shih, M.C.; Trombelli, L. Effect of lateral bone augmentation procedures in correcting peri-implant bone dehiscence and fenestration defects: A systematic review and network meta-analysis. *Clin. Implant. Dent. Relat. Res.* **2022**, *24*, 251–264. [PubMed]
5. Sheikhi, M.; Karami, M.; Abbasi, S.; Moaddabi, A.; Soltani, P. Applicability of cone beam computed tomography gray values for estimation of primary stability of dental implants. *Braz. Dent. Sci.* **2021**, *24*, 1–8.
6. Song, Y.; Yao, T.; Peng, S.; Zhu, M.; Meng, M.; Ma, J.; Zeng, D.; Huang, J.; Bian, Z.; Wang, Y. b-MAR: Bidirectional artifact representations learning framework for metal artifact reduction in dental CBCT. *Phys. Med. Biol.* **2024**, *69*, 145010. [CrossRef]
7. Ji, Y.; Zhang, J.; Hou, M.; Jin, M.; Chen, S.; Tan, J.; Zhang, X.; Wang, T. osseointegration of titanium-based and zirconia implants: Novel perspective on features, influencing factors and improvements. *J. Mater. Sci.* **2024**, *59*, 16020–16037. [CrossRef]
8. Soltani, P.; Moaddabi, A.; Mehdizadeh, M.; Bateni, M.R.; Naghdi, S.; Cernera, M.; Mirrashidi, F.; Azimipour, M.M.; Spagnuolo, G.; Valletta, A. Effect of a metal artifact reduction algorithm on cone-beam computed tomography scans of titanium and zirconia implants within and outside the field of view. *Imaging Sci. Dent.* **2024**, *54*, 313. [CrossRef]
9. Khosravifard, A.; Saberi, B.V.; Khosravifard, N.; Motallebi, S.; Kajan, Z.D.; Ghaffari, M.E. Application of an auto-edge counting method for quantification of metal artifacts in CBCT images: A multivariate analysis of object position, field of view size, tube voltage, and metal artifact reduction algorithm. *Oral Surg. Oral Med. Oral Pathol. Oral Radiol.* **2021**, *132*, 735–743. [CrossRef] [PubMed]
10. Fontenele, R.C.; Nascimento, E.H.L.; Imbelloni-Vasconcelos, A.C.; Martins, L.A.C.; Pontual, A.D.A.; Ramos-Perez, F.M.M.; Freitas, D.Q. Influence of kilovoltage-peak and the metal artifact reduction tool in cone-beam computed tomography on the detection of bone defects around titanium-zirconia and zirconia implants. *Imaging Sci. Dent.* **2022**, *52*, 267–273. [CrossRef]
11. Fontenele, R.C.; Nascimento, E.H.L.; Santaella, G.M.; Freitas, D.Q. Does the metal artifact reduction algorithm activation mode influence the magnitude of artifacts in CBCT images? *Imaging Sci. Dent.* **2020**, *50*, 23–30. [CrossRef]
12. Salib, M.; Abdalsamad, A.; Dahaba, M. Effect of metal artifacts reduction protocols and electric potential difference (kVp) on metal artifacts in cone beam computed tomography (a diagnostic accuracy study). *Egypt. Dent. J.* **2021**, *67*, 323–331.
13. Soltani, P.; Devlin, H.; Etemadi Sh, M.; Rengo, C.; Spagnuolo, G.; Baghaei, K. Do metal artifact reduction algorithms influence the detection of implant-related injuries to the inferior alveolar canal in CBCT images? *BMC Oral Health* **2024**, *24*, 268. [CrossRef]
14. Nomier, A.S.; Gaweesh, Y.S.E.; Taalab, M.R.; El Sadat, S.A. Efficacy of low-dose cone beam computed tomography and metal artifact reduction tool for assessment of peri-implant bone defects: An in vitro study. *BMC Oral Health* **2022**, *22*, 615. [CrossRef]
15. Bayrak, S.; Orhan, K.; Kursun Çakmak, E.S.; Görürgöz, C.; Odabaşı, O.; Yilmaz, D.; Atakan, C. Evaluation of a metal artifact reduction algorithm and an optimization filter in the estimation of peri-implant dehiscence defects by using cone beam computed tomography: An in-vitro study. *Oral Surg. Oral Med. Oral Pathol. Oral Radiol.* **2020**, *130*, 209–216. [CrossRef] [PubMed]

16. Soltani, P.; Devlin, H.; Aydin, U.; Tafti, K.T.; Baghaei, K. Soft tissue simulant materials in X-ray-based imaging in dentomaxillofacial radiology: A scoping review. *Oral Radiol.* **2024**, *40*, 109–123. [PubMed]
17. Freire, B.B.; Wanderley, V.A.; Câmara, J.V.F.; Santos, L.A.; Ferrari, C.R.; Araujo, T.T.; Chilvarquer, I. Effect of a metal artifact reduction algorithm on dehiscence and fenestration detection around zirconia implants with cone beam computed tomography. *Oral Surg. Oral Med. Oral Pathol. Oral Radiol.* **2024**, *138*, 316–323. [CrossRef] [PubMed]
18. Shahmirzadi, S.; Sharaf, R.A.; Saadat, S.; Moore, W.S.; Geha, H.; Tamimi, D.; Demirturk Kocasarac, H. Assessment of the efficiency of a pre- versus post-acquisition metal artifact reduction algorithm in the presence of 3 different dental implant materials using multiple CBCT settings: An in vitro study. *Imaging Sci. Dent.* **2021**, *51*, 1–7. [CrossRef] [PubMed]
19. de-Azevedo-Vaz, S.L.; Peyneau, P.D.; Ramirez-Sotelo, L.R.; Vasconcelos Kde, F.; Campos, P.S.; Haiter-Neto, F. Efficacy of a cone beam computed tomography metal artifact reduction algorithm for the detection of peri-implant fenestrations and dehiscences. *Oral Surg. Oral Med. Oral Pathol. Oral Radiol.* **2016**, *121*, 550–556. [CrossRef] [PubMed]
20. Demirturk Kocasarac, H.; Koenig, L.J.; Ustaoglu, G.; Oliveira, M.L.; Freitas, D.Q. CBCT image artefacts generated by implants located inside the field of view or in the exomass. *Dentomaxillofac. Radiol.* **2022**, *51*, 20210092. [CrossRef] [PubMed]
21. Sheikhi, M.; Behfarnia, P.; Mostajabi, M.; Nasri, N. The efficacy of metal artifact reduction (MAR) algorithm in cone-beam computed tomography on the diagnostic accuracy of fenestration and dehiscence around dental implants. *J. Periodontol.* **2020**, *91*, 209–214. [CrossRef] [PubMed]
22. Costa, J.A.; Mendes, J.M.; Salazar, F.; Pacheco, J.J.; Rompante, P.; Câmara, M.I. Analysis of peri-implant bone defects by using cone beam computed tomography (CBCT): An integrative review. *Oral Radiol.* **2023**, *39*, 455–466. [CrossRef] [PubMed]
23. Kamburoğlu, K.; Murat, S.; Kılıç, C.; Yüksel, S.; Avsever, H.; Farman, A.; Scarfe, W.C. Accuracy of CBCT images in the assessment of buccal marginal alveolar peri-implant defects: Effect of field of view. *Dentomaxillofac. Radiol.* **2014**, *43*, 20130332. [CrossRef] [PubMed]
24. Hilgenfeld, T.; Juerchott, A.; Deisenhofer, U.K.; Krisam, J.; Rammelsberg, P.; Heiland, S.; Bendszus, M.; Schwindling, F.S. Accuracy of cone-beam computed tomography, dental magnetic resonance imaging, and intraoral radiography for detecting peri-implant bone defects at single zirconia implants—An in vitro study. *Clin. Oral Implant. Res.* **2018**, *29*, 922–930. [CrossRef] [PubMed]
25. Pinheiro, L.R.; Scarfe, W.C.; de Oliveira Sales, M.A.; Gaia, B.F.; Cortes, A.R.; Gusmão Paraiso Cavalcanti, M. Effectiveness of Periapical Radiography Versus Cone Beam Computed Tomography with Different Kilovoltage Settings in the Detection of Chemically Created Peri-implant Bone Defects: An In Vitro Study. *Int. J. Oral Maxillofac. Implant.* **2017**, *32*, 741–750. [CrossRef] [PubMed]
26. Salemi, F.; Jamalpour, M.R.; Eskandarloo, A.; Tapak, L.; Rahimi, N. Efficacy of Metal Artifact Reduction Algorithm of Cone-Beam Computed Tomography for Detection of Fenestration and Dehiscence Around Dental Implants. *J. Biomed. Phys. Eng.* **2021**, *11*, 305–314. [CrossRef] [PubMed]
27. Queiroz, P.M.; Groppo, F.C.; Oliveira, M.L.; Haiter-Neto, F.; Freitas, D.Q. Evaluation of the efficacy of a metal artifact reduction algorithm in different cone beam computed tomography scanning parameters. *Oral Surg. Oral Med. Oral Pathol. Oral Radiol.* **2017**, *123*, 729–734. [CrossRef] [PubMed]